Geophysical Journal International

*Geophys. J. Int.* (2018) **213,** 2128–2137
Advance Access publication 2018 March 13
GJI Geomagnetism, rock magnetism and palaeomagnetism

doi: 10.1093/gji/ggy097

# Why magnetite is not the only indicator of past rainfall in the Chinese Loess Plateau?

Xuelian Guo,[1,2] Subir K. Banerjee,[2] Ronghua Wang,[1] Guoyong Zhao,[3] Hong Song,[1] Bin Lü,[4] Qian Li[1] and Xiuming Liu[4,5]

[1]*School of Earth Sciences, Key Laboratory of Western China's Mineral Resources of Gansu Province, Lanzhou University, Lanzhou* 730000*, China. E-mail: xlguo@lzu.edu.cn*
[2]*Institute for Rock Magnetism, University of Minnesota, Twin Cities, Minneapolis, MN* 55414*, USA*
[3]*College of Urban and Environmental Science, Xinyang Normal University, Xinyang* 464000*, China*
[4]*Research Centre of Global Change, School of Geographical Science, Fujian Normal University, Fuzhou* 350007*, China*
[5]*Department of Environment and Geography, Macquarie University, NSW* 2109*, Australia*

Accepted 2018 March 10. Received 2018 February 21; in original form 2017 November 3

## SUMMARY

This study investigates the magnetic mineralogy of palaeosol S5 from Xifeng (XF), Linyou (LY) and Baoji (BJ) sections with increasing annual precipitation from north to the south on the Chinese Loess Plateau. Palaeosol S5 samples from these three localities are further prepared as magnetic extracts and separation residues. Low-temperature magnetic measurements including field cooled and zero field cooled (FC/ZFC) remanence, in-phase magnetic susceptibility, thermal remanent magnetization and room temperature saturation isothermal remanence magnetization (RTSIRM), with X-ray diffraction measurements are carried out for all magnetic extracts and separation residues samples. The asymmetric rounded 'hump' in cooling curves on RTSIRM and the 'tilted' Verwey transition on ZFC/FC curves suggest that partially oxidized magnetite is the dominant magnetic contributor, not pure maghemite or magnetite. Furthermore, The Verwey transitions on cooling curves slightly decrease and the increased slope of 'tilted' Verwey transition on ZFC remanence curves show that the degree of oxidation of magnetite between localities increases in the order XF–LY–BJ. Hard isothermal remanent magnetization, X-ray diffraction data and the difference of magnetization in warming curves of RTSIRM suggest that both hematite concentration in magnetic extracts and goethite concentration in separation residues increase from XF to BJ. Frequency-dependent susceptibility and ZFC/FC curves show that BJS5 layer formed under high palaeoprecipitation has less superparamagnetic (SP) but more single domain to pseudo-single domain particles, because SP maghemite was dissolved and transformed into goethite by temporary waterlogging. The increase in hematite concentration is interpreted as due to SP maghemite oxidation or original goethite dehydration within dry soil environment. Therefore, transformation of maghemite to goethite in waterlogged phases of the S5 palaeosol led to the loss of magnetization.

**Key words:** Asia; Environmental magnetism; Rock and mineral magnetism.

## 1 INTRODUCTION

Magnetic mineralogy of soil and its relationship with paleoclimates have been studied over 40 yr, and the magnetic enhancement in palaeosols has proven to be very useful for paleoclimatologists to recover the paleoprecipitation (Liu *et al.* 1995; Maher *et al.* 2003; Geiss *et al.* 2008; Balsam *et al.* 2011; Orgeira *et al.* 2011; Maher & Possolo 2013; Hyland *et al.* 2015; Maxbauer *et al.* 2016). According to recent rock magnetic and mineralogical models, the superparamagnetic (SP) or single domain (SD) pedogenic maghemite/magnetite are responsible for the magnetic enhancements in palaeosols (Zhou *et al.* 1990; Liu *et al.* 1992; Banerjee *et al.* 1993; Heller *et al.* 1993; Maher & Thompson 1994; Fine *et al.* 1995; Hunt *et al.* 1995; Maher 1998; Spassov *et al.* 2003; Liu *et al.* 2005; Qiang *et al.* 2005; Nie *et al.* 2010; Zhao *et al.* 2016). Besides, pedogenic goethite, hematite, magnetite and maghemite have also been identified from magnetic characteristics (Hu *et al.* 2015) and diffuse reflectance spectroscopy (Torrent *et al.* 2007; Balsam *et al.* 2011), the ratios and contents of these magnetic minerals have certain relationship with the paleoprecipitation (Long *et al.* 2011; Orgeira *et al.* 2011; Liu *et al.* 2013).

Previous study (Orgeira *et al.* 2011) observed that relatively dry climates (<700 mm $y^{-1}$) provide the best conditions for pedogenic maghemite formation, the rate of pedogenic maghemite formation is proportional to rainfall, and do appear to show the expected increase in the values of chosen magnetic parameters (susceptibility, its frequency dependence, anhysteretic remanence, etc.). However, an increase of the mean annual rainfall is not accompanied by a proportional increase of pedogenic maghemite formation. Soils become permanently humid when rainfall increases, lacking the alternation of wet and dry conditions required for pedogenic maghemite formation, when mean annual precipitation (MAP) increases above a certain critical value (>700–1000 mm $y^{-1}$), pedogenic maghemite is destroyed by reductive dissolution (gleization), these magnetic signals begin to decrease with further increasing rainfall. They have also pointed out that the alteration and formation of different iron oxides (hematite, goethite, magnetite, maghemite) in soil depend on not simply the amount of rainfall but also the retention of moisture and pedogenic gleization.

Goethite/hematite ratio has been proposed earlier by Schwertmann and Kampf (1985) as a temperature proxy for soil of the temperate zone, and pointed to be as palaeoprecipitation indicator in soil in recent rock magnetic investigations (Long *et al.* 2011; Liu *et al.* 2013; Hyland *et al.* 2015). The frequency dependence of susceptibility to hard isothermal remanent magnetization ratio ($\chi_{fd}$/HIRM) of modern soils from Shanxi are found to have a good correlation with the modern rainfall, where $\chi_{fd}$ may be a proxy for SP magnetite/maghemite and HIRM for hematite (Liu *et al.* 2013).

This paper discusses the occurrence of magnetic minerals in loessic soils along a transect over the Chinese Loess Plateau, the relation of these minerals to climatic conditions, and the magnetic methods used for their identification. To identify the compositional variability of all the oxidized iron minerals and to estimate their amounts as accurately as possible, different methods including direct microscopic observation of thin section, scanning electron microscope and transmission electron microscope of the magnetic extracts (Chen *et al.* 2005; Yang *et al.* 2013) have been applied, and a variety of magnetic properties and their changes under different temperatures and frequencies, different methods have been tried (Zhou *et al.* 1990; Geiss & Zanner, 2006; Michal *et al.* 2010; Hu *et al.* 2015). By comparison, low-temperature measurements can lead to accurate and thermally non-destructive ways for oxidized iron minerals identification and grain-size estimates even below 20 nm.

In order to explain why high annual rainfall can lead to the loss of magnetization, and to further clarify the transformation of oxidized iron minerals in waterlogged soil environments, we collect well-developed palaeosol S5 samples from three locations (XF, LY and BJ) from more dry in the north to more humid environments in the south on the Chinese Loess Plateau. Oxidized iron minerals and grain-size of these samples are identified and estimated by using low-temperature magnetic measurements, supplemented by X-ray diffraction. Through these thermally non-destructive ways, we get accurate estimations of relative amounts of different iron oxides in S5 samples formed under different humid conditions, and discuss the relation of these minerals to climatic environments.

## 2 SAMPLES AND MEASUREMENTS

### 2.1 Sample collection

The samples for study were collected from the S5 palaeosols at the Xifeng (XF), Linyou (LY) and Baoji (BJ) sections on Chinese Loess Plateau (Guo *et al.* 2015). The present climate of the area is semi-arid to mildly humid with MAP of 550, 680 and 720 mm (up to 1100 mm in Qinling Mountain area) from XF to LY to BJ, respectively. Sixty per cent of precipitation occurs from July to September. The mean annual temperatures (MAT) are 8.7, 9.1 and 12 °C, respectively. Precipitation, which carried by the East Asian summer monsoon, decreases from south (BJ) to north (XF).

### 2.2 Magnetic extraction

Magnetic extraction of the three natural samples is carried out by using the magnetic extraction apparatus, aimed at separating strongly and weakly magnetic particles for characterization. The magnetic extraction of the bulk sample yields two subsamples: (1) mineral particles collected with an applied magnetic field, defined as the magnetic extracts (MAG), and (2) mineral particles that are non-separated fraction, defined as the residual (RES).

The magnetic extraction procedure is same in design to the pump method described by Strehlau *et al.* (2014), similar to the system described in Reynolds *et al.* (2001). A certain original S5 palaeosol sample was dispersed in 30 mL Milli-Q water using 1 g of dispersant sodium hexametaphosphate, centrifuged at 5000 rpm for 3 min using an Eppendorf 5804 centrifuge, then added to the reservoir with 200 mL Milli-Q water. The suspension was circulated by a Masterflex L/S (Cole Parmer) peristaltic pump at ∼200 mL $min^{-1}$ and passed through Tygon L/S flexible plastic tubing (Saint Gobain) oriented vertically, with a joint that contained an Nd magnet covered with a plastic sleeve to collect the magnetic material. After 90 min, the magnetic extracts were washed from the sleeve with Milli-Q water and collected for analysis. The remaining suspension in the reservoir was collected as the residues and then dried for analysis.

### 2.3 Measurements

Anhysteretic remanent magnetization (ARM) was measured in Alternating Field Demagnetizer with pARM device, the peak AF field used was 100 mT and the biasing field is 0.05 mT, ARM was then normalized by the bias field to obtain ARM susceptibility ($\chi_{ARM}$). Hysteresis loops were measured using a Princeton Measurements Vibrating Sample Magnetometer with the maximum field of 1.5 T. We used the loops' hysteresis properties to determine saturation magnetization ($M_s$), saturation remanent magnetization ($M_{rs}$), coercivity ($B_c$), remanent coercivity ($B_{cr}$), relative antiferromagnetic content (HIRM) and relative ferrimagnetic content ($S_{300}$).

A quantum design Magnetic Properties Measurement System (MPMS2) cryogenic susceptometer was used to measure cooling and warming curves of room temperature saturation isothermal remanence magnetization (RTSIRM), field cooling (FC) and zero field cooling (ZFC) remanence curves, and also for thermal remanent magnetization (TRM). SIRM produced in a 2.5 T field at 300 K was measured continuously during ZFC to 20 K at 5 K steps and back to 300 K. ZFC and FC is based on performing two consecutive magnetization measurements: In ZFC, the sample is first cooled down in the absence of a magnetic field and then measured in a 2.5 T field at increasing temperature, FC is performed in a 2.5 T field at decreasing temperature.

A second set of low-temperature measurements consisted of measuring AC susceptibility frequency- and field-dependence over the temperature range of 10–300 K at 10 K measuring steps. The in-phase susceptibility ($\chi'$) of the samples were measured in a constant 0.3 mT field and AC frequency of 1, 10 and 100 Hz, $\Delta\chi' = \chi'_{1\,\mathrm{Hz}} - \chi'_{100\,\mathrm{Hz}}$. Goethite test using low-temperature behaviour of a TRM acquired by FC from 400 to 300 K in a 0.3 mT field, and of an isothermal remanence magnetization (IRM) acquired at 300 K in a 0.3 mT field after ZFC from 400 to 300 K (Lascu & Feinberg 2011).

X-ray diffraction (XRD) patterns were obtained with a PANalytical X'pert Pro theta-theta diffractometer equipped with a Co anode and an X'celerator detector and calculate out the main oxidized iron concentrations.

## 3 RESULTS

### 3.1 Hysteresis characterization

Hysteresis loops measurements give information about the magnetic mineral composition and particle size (Evans & Heller 2003). All loops of MAG samples (Fig. 1a) close at or above 300 mT indicating the dominant presence of softer ferrimagnetic minerals such as magnetite and/or maghemite. However, the loops also show lack of complete saturation (which requires near zero slope of the loop at the highest fields) above 300 mT indicating that some harder magnetic minerals such as hematite and/or goethite may be present in MAG (Guo *et al.* 2013). The hysteresis parameters of $M_{rs}$, $B_c$, $B_{cr}$ increase monotonically from XF to BJ (Fig. 1a) pointing to increase in high-coercivity mineral such as hematite or goethite, or it could also indicate increase in SD magnetite/maghemite.

The loops of RES samples before (black curves) and after (red curves) paramagnetic correction (Fig. 1b) show the presence of softer ferrimagnetic minerals and hard magnetic minerals. Nevertheless, the $M_{rs}$ of RES are all below 0.01 $Am^2\ kg^{-1}$ (Fig. 1b), which are less than 0.4 per cent of the $M_{rs}$ of MAG (2–3 $Am^2\ kg^{-1}$, Fig. 1a), meaning that most ferrimagnetic minerals exist in the MAG samples. $B_c$ and $B_{cr}$ as concentration of hard magnetic minerals like hematite and/or goethite are usually estimated from increase in HIRM (King & Channel 1991), but hematite dominates the HIRM values (Liu *et al.* 2010; Nie *et al.* 2010). The relative abundances of soft ferrimagnetic and hard antiferromagnetic minerals are commonly quantified using the $S_{300}$ (Bloemendal *et al.* 1992; Evans & Heller 2003). From north to south, HIRMs of MAG increase from 0.025 to 0.063 and to 0.107 $Am^2\ kg^{-1}$. HIRMs of RES are around 0.00053–0.00060 $Am^2\ kg^{-1}$ with no obvious variations among three different samples. $S_{300}$ decrease from 0.98 to 0.95 to 0.93 in MAG samples, and $S_{300}$ decrease from 0.876 to 0.864 to 0.702 in the RES, respectively. Taken together, comparison of parameters $M_{rs}$, $B_c$, $B_{cr}$, HIRM, $S_{300}$ data and loops of RES samples after paramagnetic correction of the XF, LY and BJ MAG and RES samples also confirm our preliminary conclusion that hard magnetic minerals increase and relative content of soft magnetic minerals to hard magnetic minerals decrease along the transect XF–LY–BJ.

### 3.2 Low-temperature susceptibility

Examination of magnetic susceptibility as a function of temperature and field frequency has been shown to be a useful tool in distinguishing composition and grain size controls on low-temperature magnetic behaviour (Moskowitz *et al.* 1998; Brachfeld & Banerjee, 2000). The in-phase magnetic susceptibility ($\chi'$) components of the MAG fractions exhibit similar features (Fig. 2a). The MAG fractions contain magnetite as displayed by the Verwey transition (Tv $\approx$ 130 K; Banerjee *et al.* 1993), but Verwey transition in Fig. 2(a) is not sharp as for pure magnetite, the tilted straight line indicates a slight oxidation of magnetite or 'maghemite' composition, even though pure maghemite would not have displayed Verwey transition. Above Tv, most particles are SP, due to magnetic susceptibility of iron oxide minerals (such as magnetite and/or maghemite), and field frequency is inverse, so with the increasing temperature the frequency susceptibility rises, pointing to the SP fractions increase. BJS5 samples show no frequency dependence of magnetic susceptibility at any temperature (Fig. 2a), indicating minimal contents of SP grains (Brachfeld & Banerjee, 2000). By contrast, SP fractions increase from XF to LY, then decline to BJ in the MAG minerals.

The residues of XF and LY show SP presence (Fig. 2b), BJ quite different, because SP contents are very low. The sharp increased $\chi'$ components at $T < 50$ K could be due to paramagnetic clay or because of cooling below the Neel temperature of an antiferromagnetic iron silicate minerals with very little Fe.

The low-temperature difference ($\Delta\chi'$) of $\chi'$ is measured in two specific frequencies (1 and 100 Hz; Fig. 2c). The increasing $\Delta\chi'$ of MAG fractions at $T > 50$ K point to SP fraction presence. BJ shows little SP behaviour, in agreement with Figs 2(a) and (b). The $\Delta\chi'$ of three samples all drop sharply below 50 K when paramagnetic or antiferromagnetic behaviour becomes important. But comparing to MAG, the $\Delta\chi'$ of three RES samples (Fig. 2d) are near to zero, point to very low SP fractions in RES.

Clear frequency dependence susceptibility in Fig. 2 suggest that SP fractions increase from XF to LY and decline to BJ with very less SP fractions, and most of $\Delta\chi$ is carried by the MAG.

### 3.3 Mineral compositional information from cooling of RTSIRM

The room temperature remanence curves can provide estimates of oxidation from the shapes of cooling curves, and also can determine the types of magnetic minerals (Özdemir & Dunlop 2010). The Verwey transitions (Tv = ~130 K) on cooling curves (Fig. 3a) indicate the existence of magnetite in MAG samples. When temperature approaching Tv, the asymmetric rounded 'hump' in cooling curves for all three sites confirm earlier suspicion that it is oxidized magnetite (Özdemir & Dunlop 2010; Guo *et al.* 2015), not pure magnetite or pure maghemite that is the dominant magnetic carrier (Özdemir & Dunlop 2010). From the normalized comparison of warming curves (Fig. 3c) we see that BJS5-Mag shows the highest oxidation while XFS5-MAG is the lowest. Tv shows a slight decrease from 132, 131 to 126 K, indicating the oxidation degree of magnetite enhance from XF–LY–BJ (Özdemir *et al.* 1993). The presence of Morin transition of hematite at ~220 K in BJS5-MAG (Fig. 3a) shows appreciably high amount of hematite (Özdemir & Dunlop 2002) or single large hematite particles (Özdemir *et al.* 2008). It is 'appreciably high' because Morin transition is seen over and above a background of oxidized magnetite signal even though hematite magnetization is 200 times weaker (0.5 $Am^2\ kg^{-1}$ versus 93 $Am^2\ kg^{-1}$) in saturation magnetization than magnetite. There is a subtle but recognizable Morin transition at ~220 K in BJS5-RES (Fig. 3b) show a small hematite presence.

Finally, the warming curves of RES samples from all three sites (Figs 3b and d) show strong decrease between 20 and 300 K usually shown by goethite (Carter-Stiglitz *et al.* 2006). The difference of

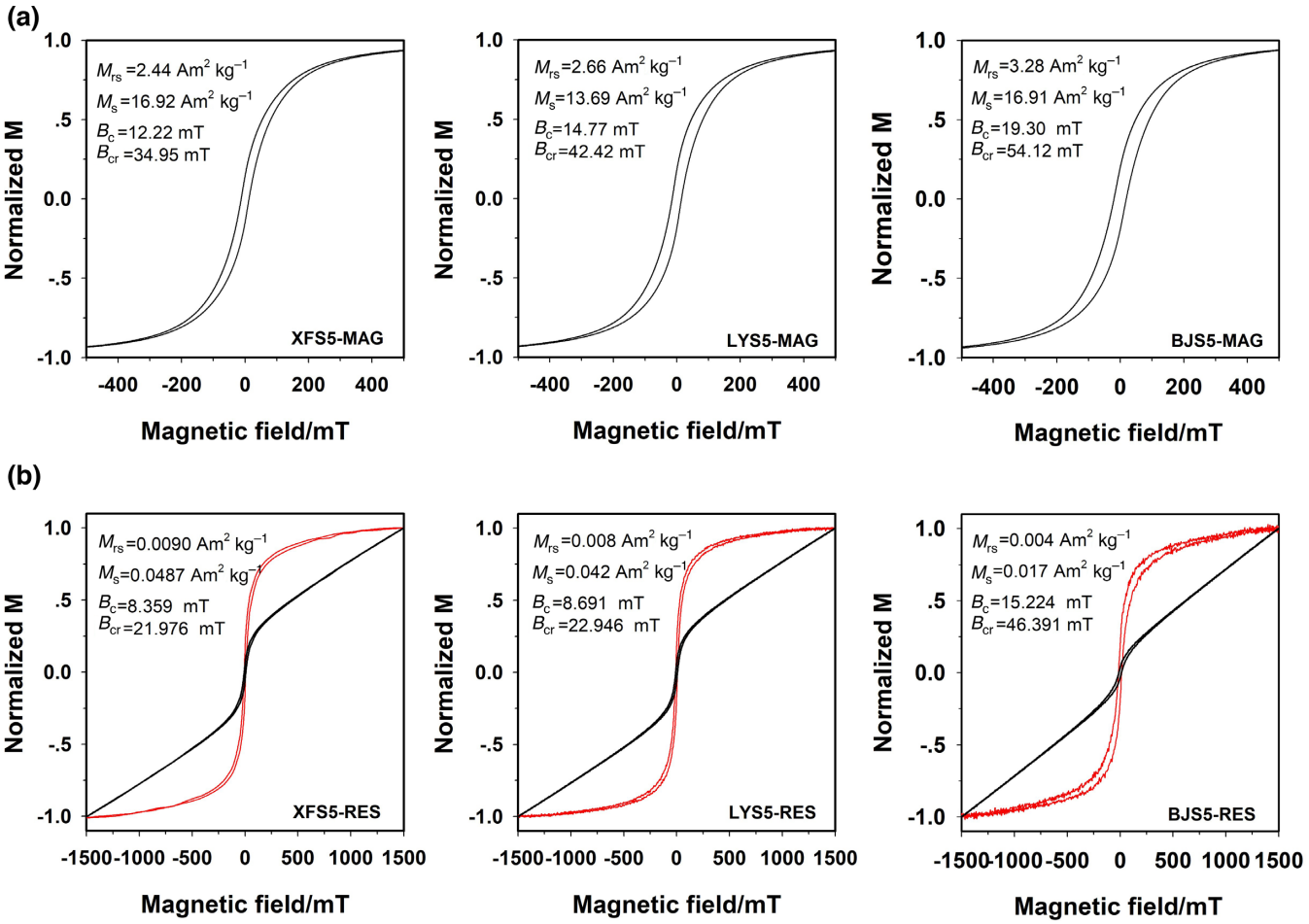


**Figure 1.** Hysteresis loops of MAG and the RES samples for the S5 transect from XF, LY and BJ. The hysteresis loops were measured in fields up to ±1.5 T to saturate ferrimagnetic magnetite and maghemite. (a) Corresponds to MAG; (b) hysteresis loops of RES before (black curves) and after (red curves) paramagnetic correction (>500 mT). The values of saturation remanence ($M_{rs}$), saturation magnetization ($M_s$), coercivity ($B_c$) and coercivity of remanence ($B_{cr}$) are listed inside the hysteresis loop plots, all values are prior to high-field slope correction.

magnetization ($\Delta M = M_{20K} - M_{300K}$) in the warming curves is 6.52, 4.84 and 3.78 × $10^{-4}$ Am$^2$ kg$^{-1}$, respectively (Fig. 3d), indicating the goethite fractions increase from XF–LY–BJ.

In all, the partially oxidized magnetite is the dominant magnetic carrier and the degree of oxidation enhance from XF–LY–BJ, BJ sample has appreciably high amount of hematite or single large hematite particles, the RES fractions show strong likelihood of goethite presence in all three sites, with the highest amount being in BJ.

### 3.4 Magnetic mineral composition and grain sizes confirmation from low temperature

Low-temperature ZFC/FC measurements were performed to further reveal the magnetic assemblage in the samples (Brachfeld & Banerjee 2000). The tilted Verwey transition at ∼120 K on ZFC/FC curves (Fig. 4a) point to the presence of partially oxidized magnetite, not pure magnetite in XF, LY and BJ MAG samples. From the normalized comparison of ZFC remanence curves (Fig. 4c) we see that the slope of 'tilted' Verwey transition increase from XF–LY–BJ indicating the oxidation degree of magnetite enhanced. These further confirm RTSIRM results that it is partially oxidized magnetite, not pure magnetite or pure maghemite that is the dominant magnetic carrier. Moreover, FC curve has higher values than ZFC curve (Fig. 4a) indicating SD and/or PSD behaviour, not large particles (>10 $\mu$m) in magnetic separates, SD/PSD are the mainly magnetic particles. In contrast, ZFC curves of three RES samples (Fig. 4b) without obvious Verwey transition at ∼120 K show that the particles are oxidized and finer (more SP) grains, the steep temperature-dependence curves suggest the presence of high coercivity, magnetically unsaturated goethite in the RES (Guyodo *et al.* 2003; Carter-Stiglitz *et al.* 2006). The remanence loss is approximately 67 per cent, 66 per cent and 60 per cent of the initial remanence for XF, LY and BJ RES samples (Fig. 4d), suggesting SP fractions are more in XF and LY than in BJ, and show a slightly decrease upon going from XF–LY–BJ.

Overall, the oxidized magnetite is the main magnetic carrier in MAG and the oxidation degree enhance from XF–LY–BJ. In addition, more goethite present in RES. By contrast, BJS5 sample has minimal SP fractions. This consistent with the RTSIRM characters (Fig. 3) and in-phase susceptibility ($\chi'$) results (Fig. 2).

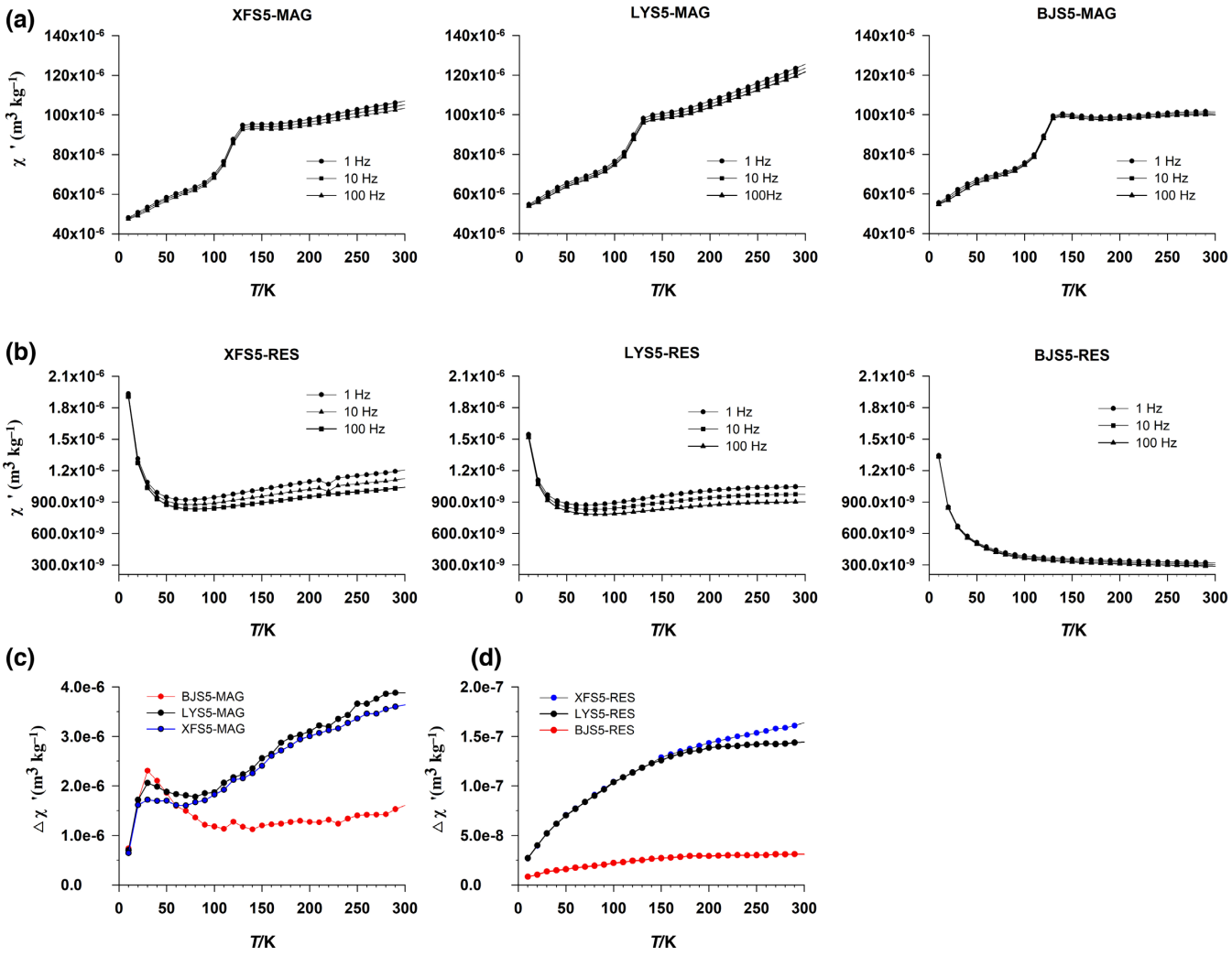


**Figure 2.** Low-temperature variations of in-phase magnetic susceptibility ($\chi'$) for field frequencies of 1, 10 and 100 Hz for MAG samples (a) and RES samples (b) from XF, LY and BJ. Low-temperature difference ($\Delta\chi'$) of frequency dependence $\chi'$ in two specific frequencies (1 and 100 Hz) from MAG samples (c) and RES samples (d) from XF, LY and BJ.

### 3.5 Oxidized iron concentrations in magnetic extracts

In order to quantify the amount of oxidized iron minerals we measured MAG samples using XRD, the results are shown in Fig. 5. XFS5-MAG has the least hematite and the highest magnetite concentrations. LYS5-MAG has the same magnetite and maghemite concentrations as BJS5-MAG and intermediate amounts of hematite. BJS5-MAG has the highest hematite concentration, which is about 2.7 times higher than magnetite or maghemite concentration. The total concentration of magnetite + maghemite (57.6 per cent, 47.0 per cent, 41.7 per cent, respectively) decline from XF–LY–BJ. Hematite concentration increases from XF–LY–BJ, which quantitatively confirms the above results of RTSIRM, FC/ZFC and hysteresis data. Hematite have maximum contents in MAG samples, by contrast, goethite concentration is very low in all MAG samples (Fig. 5), a reasonable explanation could be fine hematite particles often appeared on the edge and surface of ferrimagnetic minerals and extracted easily (Hu *et al.* 2013), the most of goethite concentration still left in the residues.

### 3.6 Goethite test in separation residues

Goethite was identified using a rock magnetic test to target this mineral (Lascu & Feinberg 2011), and this approach is similar to that of demagnetizing the low coercivity minerals employed by Guyodo *et al.* (2006). Curve **a** of Fig. 6 is the ZFC from 300 to 20 K, the magnetization increase and Verwey transition at ∼120 K confirm the presence of magnetite. Above Tv, the increasing magnetization show existence of high coercivity goethite. Curve **b** linearly drop from 20 to 400 K shows the presence of goethite. Both IRM cooling and warming curves (**c**, **d**) in a 0.3 T field display low coercivity magnetite character because goethite has very little remanence in 0.3 T field. The overlap of **e** and **f** curves confirm the presence of goethite in BJS5-RES sample, the difference at room temperature between the total magnetization and remainder was taken to represent the concentration of goethite in the BJS5-RES sample.

## 4 DISCUSSION

We have studied S5-1 palaeosol from the Chinese Loess Plateau and suggested that pedogenesis and chemical weathering of the coeval S5-1 palaeosol layers increased from north to south from

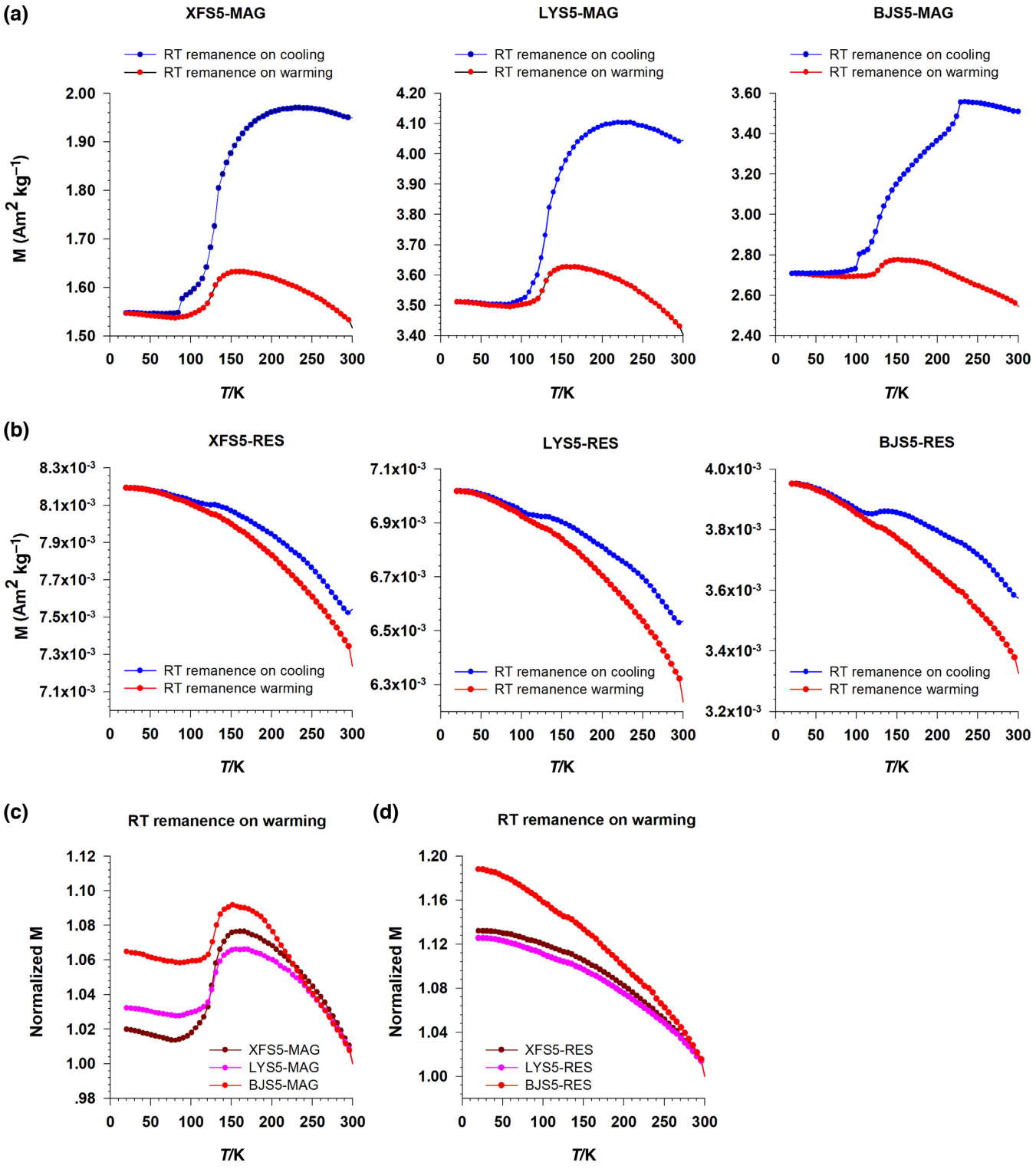


**Figure 3.** RTSIRM produced in a 2.5 T field at 300 K was measured continuously during zero field cooling to 20 K at 5 K steps and back to 300 K. Panel (a) displays cooling and warming back of RTSIRM of MAG of S5 palaeosols from XF, LY and BJ. Panel (b) shows the same type of data for the RES from S5 palaeosol from XF, LY and BJ. Panel (c) displays normalized RTSIRM on warming of MAG and panel (d) shows normalized RTSIRM on warming of RES of S5 palaeosols from XF, LY and BJ. Imparting a high field SIRM to a sample containing magnetite or oxidized magnetite at room temperature and then cycling the remanence in zero fields from 300 to 20 to 300 K can be a very effective and non-destructive technique for identifying the compositions.

localities XF to BJ. Some fine-grained strongly magnetic minerals were converted into weakly magnetic minerals (mainly hematite and goethite) by pedogenesis, which resulted in a decline in SP and stable single domain (SSD) ferrimagnetic minerals and decreasing susceptibility of S5-1 palaeosol from north to south(Guo *et al.*

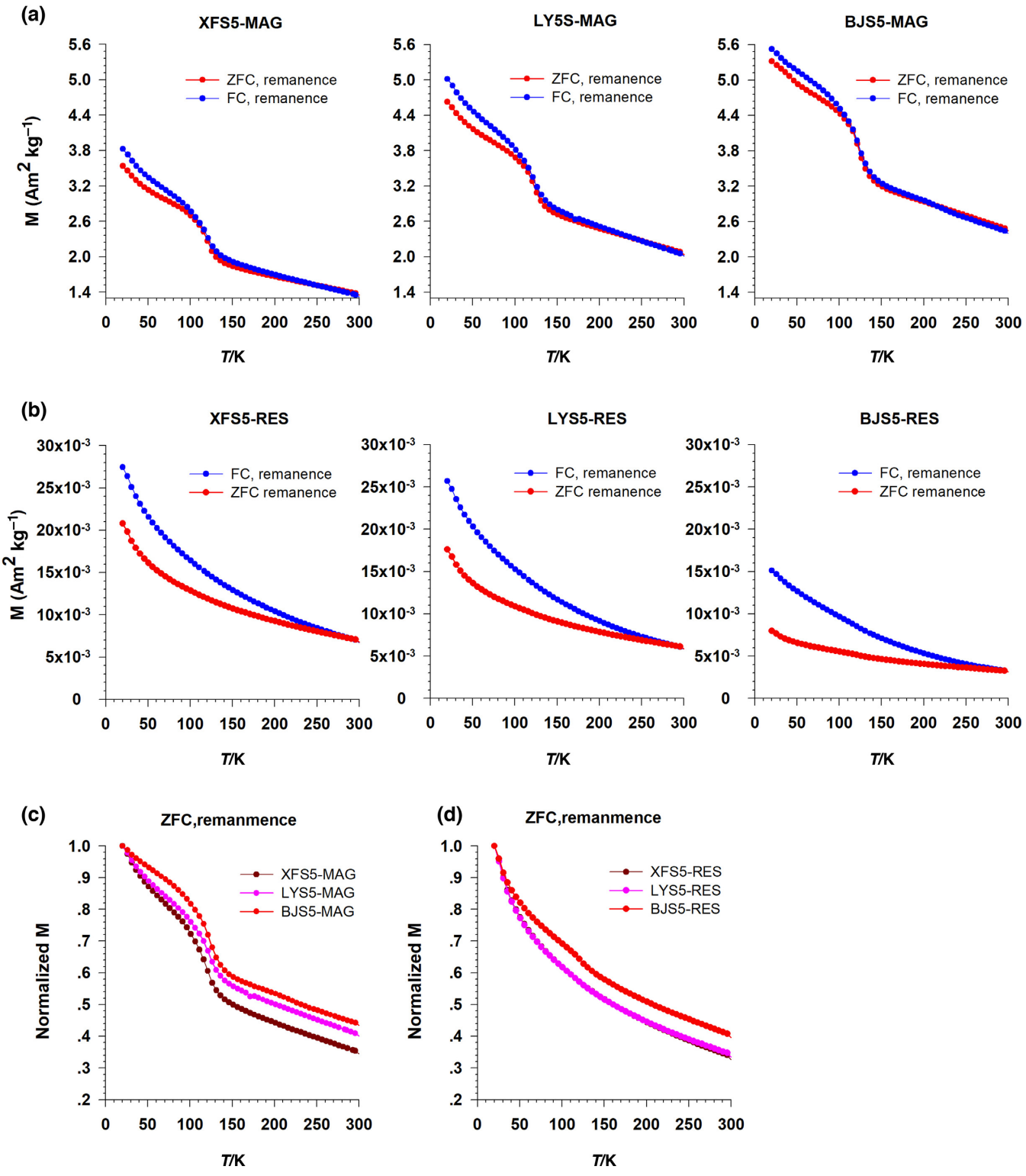


**Figure 4.** Low-temperature field cooled (FC) and zero field cooled (ZFC) remanent magnetization acquired at 20 K in 2.5 T field from 300 to 20 K in MAG (a) and RES (b) from palaeosol S5 from XF, LY and BJ. (c) and (d) show normalized ZFC remanent magnetization in MAG and RES from palaeosol S5 from XF, LY and BJ.

2015). We used low-temperature magnetism and XRD to quantitatively examine how high annual rainfall in Chinese Loess Plateau leads to loss of magnetization, and further clarify the transformation of oxidized iron in waterlogged soil environments from XF to BJ.

### 4.1 The compositional variability of the oxidized iron minerals from XF–LY–BJ in Chinese Loess Plateau

According to above low-temperature magnetic behaviour (RT-SIRM, $\chi'$, FC/ZFC), we find that magnetic minerals in S5 palaeosol

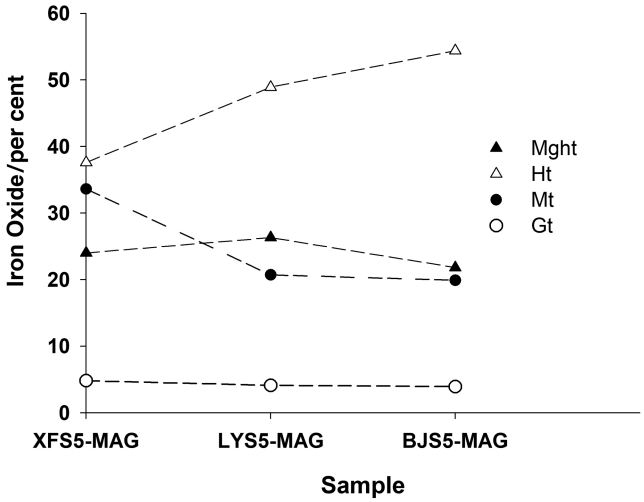


**Figure 5.** Magnetic oxidized iron concentration of MAG acquired by XRD. Mght, maghemite; Ht, hematite; Mt, magnetite; Gt, geothite.

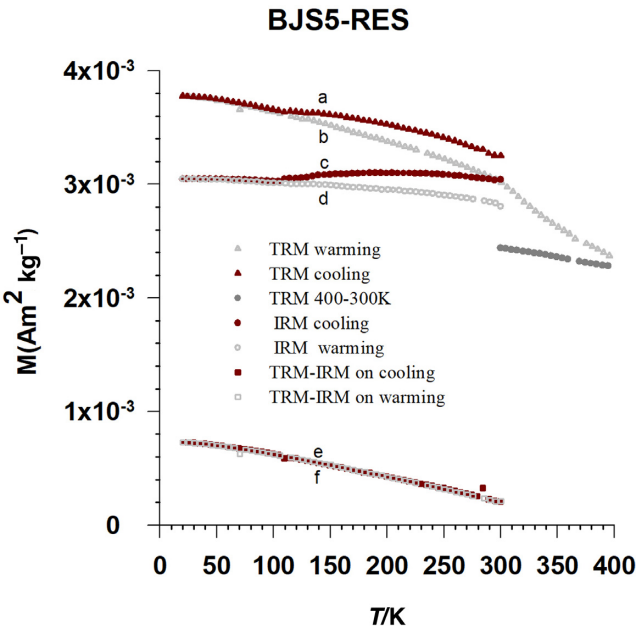


**Figure 6.** Low-temperature behaviour of a TRM (**a** and **b**, triangles) acquired by field cooling (FC) from 400 to 300 K in a 0.3 T field, and of an IRM (**c** and **d**, circles) acquired at 300 K in a 0.3 T field after zero-field cooling (ZFC) from 400 to 300 K, the separation of the curves above ∼120 K (Verwey transition, Tv) is diagnostic of magnetite. The difference (squares) between the TRM and IRM warming (**e**, square, grey) and cooling (**f**, square, red) curves respectively is a measure of the presence of goethite, which acquires remanence during the FC pre-treatment and is demagnetized during the ZFC pre-treatment (Guyodo *et al.* 2006; Lascu & Feinberg 2011).

are oxidized-magnetite, maghemite, hematite and goethite. Hysteresis parameters $B_c$, $B_{cr}$ and HIRM increase monotonically from XF–LY–BJ (Fig. 1). but $S_{300}$ and the total concentration of magnetite + maghemite (Fig. 5) decline over the same environmental transect, implying to hard magnetic mineral concentrations increase, and relative concentrations of soft magnetic minerals descend along the transect XF–LY–BJ. The asymmetric rounded 'hump' in cooling curves on RTSIRM (Figs 3a and c) and the 'tilted' Verwey transition on ZFC/FC curves (Fig. 4) suggest that partially oxidized magnetite, neither pure magnetite nor pure maghemite, is the dominant magnetic carrier. Low-temperature magnetic properties are in agreement with magnetic hysteresis parameters, the partially oxidized magnetite in SD–PSD ranges can reliably record paleomagnetic signals (Ge *et al.* 2014). From the normalized comparison of cooling curves on RTSIRM we see that Tv slightly decrease from 132, 131 to 126 K (Fig. 3c), and the increased slope of 'tilted' Verwey transition of ZFC remanence curves (Fig. 4c) from XF–LY–BJ show that the oxidation degree of magnetite enhance with increasing MAT (8.7 °C, 9.1 °C to 12 °C) from north to south. The ratios of FeD/FeT, elements' concentrations and redness values also confirm that pedogenic degree enhances from north to south in Chinese Loess Plateau (Hao & Guo 2005; Guo *et al.* 2015).

The steep temperature-dependent ZFC/FC curves (Fig. 4b) and RTSIRM on warming curves of Res samples (Figs 3b and d) indicate the presence of goethite, we also measured BJS5-RES by low-temperature behaviour of TRM and IRM (Fig. 6), The overlap of the difference between the TRM and IRM warming (Fig. 6e, square, grey) and cooling (Fig. 6f, square, red) curves further confirm the presence of goethite (Lascu & Feinberg 2011). Simultaneously, the $\Delta M$ ($\Delta M = M_{20K} - M_{300K}$) in warming curves of RTSIRM (Fig. 3d) show the goethite fractions increase from XF to BJ. These are consistent with the field observations: no Fe–Mn coatings were seen in XF S5 palaeosol layer, and only a little amount of Fe–Mn coatings in LY S5 palaeosol layer, and abundant Fe–Mn coatings in BJ S5 palaeosol layer (Guo *et al.* 2015).

The Morin transition of hematite at ∼220 K in BJS5-MAG and BJS5-RES (Figs 3a and b) show appreciably high hematite concentration or single large hematite particles (Özdemir *et al.* 2008). But XRD data quantitatively suggest hematite concentration are 2.7 times higher than magnetite, maghemite and geothite concentrations in MAG samples for all three sections and rapidly increase with increasing MAP from XF to BJ (Fig. 5), HIRM data (from 0.025 and 0.063 to 0.107 $Am^2\ kg^{-1}$) of MAG also confirm this interpretation. HIRM of RES are 0.00055, 0.00053 and 0.00060 $Am^2\ kg^{-1}$ with no obvious variations among three different samples, this confirm that hematite dominates the HIRM value (Liu *et al.* 2010; Nie *et al.* 2010). All suggest that hematite concentration of BJS5-MAG is indeed high, a reasonable explanation could be its fine particles often appeared on the edge and surface of ferrimagnetic minerals and extracted easily (Hu *et al.* 2013).

From XF to LY with low MAP (which was 550 and 680 mm), magnetite was oxidized to maghemite during pedogenesis, maghemite continued to be oxidized to hematite under dry conditions (Liu *et al.* 2008). Thus magnetite concentration declines, and maghemite and hematite concentrations go up from XF to LY. From LY to BJ (modern MAP from 680 to 720 mm), pedogenesis occurred intermittently between wet and dry conditions. In water-logged soil environments, fine-grain maghemite dissolved releasing $Fe^{3+}$, and goethite was precipitated (Schwertmann & Murad 1983). The increase of hematite concentration with increasing precipitation from XF to BJ is due to dehyrdation of original goethite or oxidation of maghemite. While maghemite concentration displays a little reduction, due to pedogenic maghemite is destroyed under reducing conditions during the wetting phase (Orgeira *et al.* 2011). In humid climates where MAP exceeds ∼1000 mm $y^{-1}$, modern soil shows that negative correlations between MAP and magnetic enhancement parameters (Balsam *et al.* 2011; Long *et al.* 2011). This is attributed to the increased dissolution of iron oxides and leaching that persists in water-saturated soil with only limited dry periods (Maher 2011; Orgeira *et al.* 2011).

### 4.2 The compositional variability of pedogenic magnetic particles from oxidizing to weakly reducing environments

Frequency dependent susceptibility $\chi'$ curves (Fig. 2) show that SP particles are more abundant in XF and LY samples than in BJ. Great FC than ZFC magnetization below the Verwey transition (Fig. 4) is indicative of an SD to PSD dominated magnetite grain size distribution. Moreover, the low-temperature frequency susceptibility $\chi'$–$T$ curves (Fig. 2) show SP composition slightly increases from XF to LY and then rapidly decline to BJ, with very low SP compositions in BJ S5 sample. Likewise, as an extremely sensitive indicator for SSD particles (King & Channell 1991), the $\chi_{ARM}$ of MAG are 1.95, 1.93 and 1.75 $\times$ $10^{-4}$ $m^3$ $kg^{-1}$ among XFS5-MAG, LYS5-MAG and BJS5-MAG samples, the $\chi_{ARM}$ of BJS5-RES (9.3 $\times$ $10^{-5}$ $m^3$ $kg^{-1}$) is higher than XFS5-RES (6.5 $\times$ $10^{-6}$ $m^3$ $kg^{-1}$) and LYS5-RES (5.5 $\times$ $10^{-6}$ $m^3$ $kg^{-1}$) in RES samples. In all, the SP composition increases and SD/PSD composition decreases from XF to LY, because with increasing pedogenesis the magnetite was oxidized to maghemite and hematite, while BJS5 has much more SD/PSD particles, very less SP particles. This may be because SP maghemite was dissolved, and recrystallized into goethite under temporary waterlogging caused by abundant rainfall in BJS5 palaeosol. This is compatible with the observation of Smirnov & Tarduno (2000), who suspected selective elimination of small grains first. The dissolution of magnetic minerals commonly occurs in weakly reducing or gleyed environments (Liu *et al.* 2008).

## 5 CONCLUSIONS

Low-temperature magnetic measurements and XRD study of MAG and RES from XF, LY and BJ S5 palaeosols show that:

(1) The oxidized magnetite, not pure maghemite or pure magnetite, is the main magnetic carrier in S5 palaeosols, and the oxidation degree of magnetite enhances along section from XF–LY–BJ.

(2) Both hematite concentration of MAG and goethite concentration of RES increase with increasing MAP from XF to BJ. The rapid increase of hematite concentration is interpreted as previously formed goethite dehydration or SP maghemite oxidized within dry soil environment.

(3) The SP concentration increases and SD/PSD concentration decreases from XF to LY because with increasing pedogenesis the magnetite was oxidized to maghemite and hematite, while BJS5 has much more SD/PSD particles, very less SP particles, due to SP maghemite was dissolved and transformed into goethite under temporary waterlogging caused by abundant rainfall, which resulted in goethite concentration increasing.

## SUPPORTING INFORMATION

Supplementary data are available at *GJI* online.

**Table.** Hysteresis parameters of MAG and RES samples before high-field slope correction.

Please note: Oxford University Press is not responsible for the content or functionality of any supporting materials supplied by the authors. Any queries (other than missing material) should be directed to the corresponding author for the paper.

## ACKNOWLEDGEMENTS

The low-temperature magnetic measurements were made at the Institute for Rock Magnetism (IRM), University of Minnesota. XRD was measured at Department of Chemistry, University of Minnesota. We thank Mike Jackson, Dario Bilardello and Peat Sølheid of IRM for their help with the experiments, and thank Prof. R. Lee Penn and Ph.D. Alex Henrique Pinto of Department of Chemistry, University of Minnesota, for their help with the XRD measurements. The IRM is supported by US National Foundations EAR/IF division and the University of Minnesota. This is IRM contribution no.1605. This research was supported by the National Natural Science Foundation of China (grant nos. 41772168, 41772180, 41402147, 41402149 and 41602187), XG was further supported by Scientific Research Foundation for the Returned Overseas Chinese Scholars, Gansu Province.

## REFERENCES

Balsam, W.L., Ellwood, B.B., Ji, J.F., Williams, E.R., Long, X.Y. & Hassani, A.E., 2011. Magnetic susceptibility as a proxy for rainfall: worldwide data from tropical and temperate climate, *Quat. Sci. Rev.,* **30,** 2732–2744.

Banerjee, S.K., Hunt, C.P. & Liu, X.M., 1993. Separation of local signals from the regional paleomonsoon record of the Chinese Loess Plateau: a rock-magnetic approach, *Geophys. Res. Lett.,* **20**(9), 843–846.

Bloemendal, J., King, J.W., Hall, F.R. & Doh, S.J., 1992. Rock magnetism of Late Neogene and Pleistocene deep-sea sediments: relationship to sediment source, diagenetic processes, and sediment lithology, *J. geophys. Res.,* **97,** 4361–4375.

Brachfeld, S. A. & Banerjee, S.K., 2000. Rock-magnetic carriers of century-scale susceptibility cycles in glacial-marine sediments from the Palmer Deep, Antarctic Peninsula, *Earth planet. Sci. Lett.,* **176,** 443–455.

Carter-Stiglitz, B., Moskowitz, B., Solheid, P., Berquó, T.S., Jackson, M. & Kosterov, A., 2006. Low-temperature magnetic behavior of multi domain titanomagnetites: TM0, TM16, and TM35, *J. geophys. Res.,* **111**(B12).

Chen, T.H., Xu, H.F., Xie, Q.Q., Chen, J., Ji, J.F. & Lu, H.Y., 2005. Characteristics and genesis of maghemite in Chinese loess and paleosols: mechanism for magnetic susceptibility enhancement in paleosols, *Earth planet. Sci. Lett.* **240,** 790–802.

Evans, M.E. & Heller, F., 2003. *Environmental Magnetism: Principles and Applications of Enviromagnetics,* Academic Press, pp. 1–299.

Fine, P., Verosub, K.L. & Singer, M.J., 1995. Pedogenic and lithogenic contributions to the magnetic susceptibility record of the Chinese loess/paleosol sequence, *Geophys. J. Int.,* **122,** 97–107.

Ge, K.P., Williams, W., Liu, Q.S. & Yu, Y.J., 2014. Effects of the core-shell structure on the magnetic properties of partially oxidized magnetite grains: experimental and micromagnetic investigations, *Geochem. Geophys. Geosyst.,* **15,** 2021–2038.

Geiss, C.E. & Zanner, C.W., 2006. How abundant is pedogenic magnetite? Abundance and grain size estimates for loessic soils based on rock magnetic analyses, *J. geophys. Res.,* **111,** B12S21

Geiss, C.E., Egli, R. & Zanner, C.W., 2008. Direct estimates of pedogenic-magnetite as a tool to reconstruct past climates from buried soils, *J. geophys. Res.,* **113,** B11102.

Guo, X.L., Liu, X.M., Li, P.Y., Lü, B., Guo, H., Chen, Q. & Ma, M.M., 2013. The magnetic mechanism of paleosol S5 in the Baoji section of the southern Chinese Loess Plateau, *Quat. Int.,* **306,** 129–136.

Guo, X.L., Liu, X.M., Miao, S. J., Zhao, G.Y. & Liu, Y.X., 2015. Variability of magnetic character of S5-1 paleosol (age ~ 470 Ka) along a rainfall transect explains why susceptibility decreased with high rainfall, *Aeolian Res.*, **19,** 55–63.

Guyodo, Y., Mostrom, A., Lee, P.R. & Banerjee, S.K., 2003. From nanodots to nanorods: Oriented aggregation and magnetic evolution of nanocrystalline goethite, *Geophys. Res. Lett.,* **30,** 19–11.

Guyodo, Y., Banerjee, S.K., Lee, P.R., Burleson, D., Berquo, T.S., Seda, T. & Solheid, P., 2006. Magnetic properties of synthetic six-line ferrihydrite nanoparticles, *Phys. Earth planet. Inter.,* **154,** 222–233.

Hao, Q.Z. & Guo, Z.T., 2005. Spatial variations of magnetic susceptibility of Chinese loess for the last 600 kyr: implications for monsoon evolution, *J. geophys. Res.* **110,** B12101.

Heller, F., Shen, C.D., Beer, J., Liu, X.M., Liu, T.S., Bronger, A., Suter, M. & Bonani, G., 1993. Quantitative estimates of pedogenic ferromagnetic mineral formation in Chinese loess and palaeoclimatic implications, *Earth planet. Sci. Lett.,* **114,** 385–390.

Hu, P.X., Liu, Q.S., Torrent, J., Barrón, V. & Jin, C.S., 2013. Characterizing and quantifying iron oxides in Chinese loess/paleosols: implications for pedogenesis, *Earth planet. Sci. Lett.,* **369–370,** 271–283.

Hu, P.X., Liu, Q.S., Heslop, D., Roberts, A. P. & Jin, C.S., 2015. Soil moisture balance and magnetic enhancement in loess–paleosol sequences from the Tibetan Plateau and Chinese Loess Plateau, *Earth planet. Sci. Lett.,* **409,** 120–132.

Hunt, C.P., Banerjee, S.K., Han, J.M., Solheid, P.A., Oches, E., Sun, W.W. & Liu, T.S., 1995. Rock magnetic proxies of climate change in the loess-paleosol sequences of the western Loess Plateau of China, *Geophys. J. Int.,* **123,** 232–244.

Hyland, E., Sheldon, N.D., Van der Voo, R., Badgley, C. & Abrajevitch, A., 2015. A new paleoprecipitation proxy based on soil magnetic properties: implications for expanding paleoclimate reconstructions, *Bull. geol. Soc. Am.,* **127**(7), 975–981.

King, J. & Channell, J., 1991. Sedimentary magnetism, environmental magnetism and magneto-stratigraphy, 1987–1990, *Rev. Geophys.,* **39,** 358–370.

Lascu, I. & Feinberg, J. M., 2011. Speleothem magnetism, *Quat. Sci. Rev.,* **30,** 3306–3320.

Liu, Q.S., Torrent, J., Maher, B.A., Yu, Y.J., Deng, C.L., Zhu, R.X. & Zhao, X.X., 2005. Quantifying grain size distribution of pedogenic magnetic particles in Chinese loess and its significance for pedogenesis, *J. geophys. Res.,* **110,** B11102.

Liu, Q.S., Barrón, V., Torrent, J., Eeckhout, S.G. & Deng, C.L., 2008. Magnetism of intermediate hydromaghemite in the transformation of 2-line ferrihydrite into hematite and its paleoenvironmental implications, *J. geophys. Res.,* **113,** B01103. .

Liu, Q.S., Hu, P.X., Torrent, J., Barrón, V., Zhao, X.Y., Jiang, Z.X. & Su, Y.L., 2010. Environmental magnetic study of a Xeralf chronosequence in northwestern Spain: indications for pedogenesis, *Palaeogeogr. Palaeoclimatol. Palaeoecol.,* **293,**144–156.

Liu, X.M., Shaw, J., Liu, T.S., Heller, F. & Yuan, B.Y., 1992. Magnetic mineralogy of Chinese loess and its significance, *Geophys. J. Int.,* **108,** 301–308.

Liu, X.M., Rolph, T., Bloemendal, J., Shaw, J. & Liu, T.S., 1995. Quantitative estimates of paleoprecipitation at Xifeng in the loess plateau of China, *Palaeogeogr. Palaeoclimatol. Palaeoecol.,* **113,** 243–248.

Liu, Z.F., Liu, Q. S., Torrent, J., Barrónc, V. & Hu, P.X., 2013. Testing the magnetic proxy $\chi_{FD}$/HIRM for quantifying paleorainfall in modern soil profiles from Shaanxi Province, China, *Glob. Planet. Change,* **110,** 368–378.

Long, X., Ji, J. & Balsam, W., 2011. Rainfall-dependent transformations of iron oxides in a tropical saprolite transect of Hainan Island, South China: spectral and magnetic measurements, *J. geophys. Res.,* **116,** F03015.

Maher, B.A., 1998. Magnetic properties of modern soils and quaternary loessic paleosols: paleo-climatic implications, *Palaeogeogr. Palaeoclimatol. Palaeoecol.,* **137,** 25–54.

Maher, B.A., 2011. The magnetic properties of Quaternary aeolian dusts and sediments, and their palaeoclimatic significance, *Aeolian Res*., **3,** 87–144.

Maher, B.A. & Possolo, A., 2013. Statistical models for use of palaeosol magnetic properties as proxies of palaeorainfall, *Glob. Planet. Change,* **111,** 280–287.

Maher, B.A. & Thompson, R., 1994. Comments on: pedogenesis and paleoclimate interpretation of the magnetic susceptibility record of Chinese loess-paleosol sequences, *Geology,* **23,** 857–858.

Maher, B.A., Alekseev, A. & Alekseeva, T., 2003. Variation of soil magnetism across the Russian steppe: its significance for use of soil magnetism as a palaeorainfall proxy, *Quat. Sci. Rev.* **21,** 1571–1576.

Maxbauer, D.P., Feinberg, J.M. & Fox, D.L., 2016. Magnetic mineral assemblages in soils and paleosols as the basis for paleoprecipitation proxies: a review of magnetic methods and challenges, *Earth-Sci. Rev*., **155,** 28–48.

Michel, F.M., Barron, V., Torrent, J., Morales, M.P., Serna, C.J., Boily, J.F., Liu, Q.S., Ambrosini, A., Cismasu, A.C. & Brown, G.E., 2010. Ordered ferrimagnetic form of ferrihydrite reveals links among structure, composition, and magnetism, *Proc. Natl. Acad. Sci. USA,* **107,** 2787–2792.

Moskowitz, B.M., Jackson, M. & Kissel, C., 1998. Low-temperature magnetic behavior of titanomagnetites, *Earth planet. Sci. Lett.,* **157,** 141–149.

Nie, J.S., Song, Y.G., King, J.W., Fang, X.M. & Heil, C., 2010. HIRM variations in the Chinese red-clay sequence: insights into pedogenesis in the dust source area, *J. Asian Earth Sci.,* **38,** 96–104.

Orgeira, M.J., Egli, R. & Compagnucci, R.H., 2011. A quantitative model of magnetic enhancement in loessic soils, in *The Earth's Magnetic Interior,* pp. 361–397, eds , ,Petrovsky, E. , ,Ivers, D. ,Harinarayana, T. & Herrero-Bervera,, E., Springer.

Özdemir, Ö. & Dunlop, D.J., 2002. Thermoremanence and stable memory of single-domain hematites, *Geophys. Res. Lett.,* **29**(18), 24–21.

Özdemir, Ö. & Dunlop, D.J., 2010. Hallmarks of maghemitization in low-temperature remanence cycling of partially oxidized magnetite nanoparticles, *J. geophys. Res.,* **115,** B02101.

Özdemir, Ö., Dunlop, D.J. & Moskowitz, B.M., 1993. The effect of the Verwey transition in magnetite, *Geophys. Res. Lett.,* **20,** 1671–1674.

Özdemir, Ö., Dunlop, D.J. & Berquó, T.S., 2008. Morin transition in hematite: Size dependence and thermal hysteresis, *Geochem. Geophys. Geosyst.,* **9,** .

Qiang, X.K., An, Z.S., Li, H.M., Chang, H. & Song, Y.G., 2005. Magnetic properties of Jiaxian red clay sequences from northern Chinese Loess Plateau and its paleoclimatic significance, *Sci. China Earth Sci.,* **48,** 1234–1245.

Reynolds, R.L., Sweetkind, D.S. & Axford, Y., 2001. An inexpensive magnetic mineral separator for fine-grained sediment: U.S. Geological Survey, Open-File Report, 1–281, 7 p,

Schwertmann, U. & Kämpf, N., 1985. Properties of goethite and hematite in kaolinitic soils of southern and central Brazil, *Soil Sci*., **139,** 344–350.

Schwertmann, U. & Murad, E., 1983. Effect of pH on the formation of goethite and hematite from ferrihydrite, *Clays Clay Miner*., **31,** 277–284.

Smirnov, A.V. & Tarduao, J.A., 2000. Low-temperature magnetic properties of pelagic sediments (Ocean Drilling Program site 805C): tracers of magnemitization and magnetic mineral reduction, *J. geophys. Res.,* **105,** 16 457–16 471.

Spassov, S., Heller, F., Kretzschmar, R., Evans, M.E., Yue, L.P. & Nourgaliev, D.K., 2003. Detrital and pedogenic magnetic mineral phases in the loess/palaeosol sequence at Lingtai (central Chinese Loess Plateau), *Phys. Earth planet. Inter.,* **140,** 255–275.

Strehlau, J.H., Hegner, L.A., Strauss, B.E., Feinberg, J.M. & Penn, R.L., 2014. Simple and efficient separation of magnetic minerals from speleothems and other carbonates, *J. Sediment. Res.,* **84,** 1096–1106.

Torrent, J., Liu, Q.S., Bloemendal, J. & Barrón, V., 2007. Magnetic enhancement and iron oxides in the upper Luochuan loess–paleosol sequence, Chinese Loess Plateau, *Soil Sci. Soc. Am. J.,* **71,** 1570–1578.

Yang, T.S., Hyodo, M., Zhang, S.H., Maeda, M., Yang, Z.Y., Wu, H.C. & Li, H.Y., 2013. New insights into magnetic enhancement mechanism in chinese paleosols, *Palaeogeogr. Palaeoclimatol. Palaeoecol.,* **369**(1), 493–500.

Zhao, G.Y., Han, Y., Liu, X.M., Chang, L., Lü, B., Chen, Q., Guo, X.L. & Yan, J.H., 2016. Can the magnetic susceptibility record of Chinese Red Clay sequence be used for palaeomonsoon reconstructions ? *Geophy. J. Int.,* **204,** 1421–1429.

Zhou, L.P., Oldfield, F., Wintle, A.G., Robinson, S.G. & Wang, J.T., 1990. Partly pedogenic origin of magnetic variations in Chinese loess, *Nature,* **346,** 737–739.